Applied Catalysis B: Environmental 313 (2022) 121435

Contents lists available at ScienceDirect

Applied Catalysis B: Environmental

journal homepage: www.elsevier.com/locate/apcatb

Identifying the realistic catalyst for aqueous phase reforming of methanol over Pt supported by lanthanum nickel perovskite catalyst

Qianlong Mao [a], Yong Guo [a,*], Xiaohui Liu [a], Mohsen Shakouri [b], Yongfeng Hu [b], Yanqin Wang [a]

[a] Shanghai Key Laboratory of Functional Materials Chemistry, Research Institute of Industrial Catalysis, School of Chemistry and Molecular Engineering, East China University of Science and Technology, Shanghai 200237, PR China
[b] Canadian Light Source Inc., 44 Innovation Boulevard, Saskatoon, SK, Canada S7N 2V3

ARTICLE INFO

Keywords:
Hydrogen production
Aqueous phase reforming
Perovskite
Pt
$LaCO_3OH$

ABSTRACT

In-situ supply of H_2 by aqueous phase reforming (APR) of methanol is promising but still challenging due to the unsatisfied activity and stability of catalyst. Herein, we prepared lanthanum nickel perovskite supporting Pt catalysts and evaluated their performance in methanol APR. A transformation from lanthanum nickel perovskite into $LaCO_3OH$ happened after APR. The characterizations results reveal that these two perovskite catalysts transformed into $LaCO_3OH$ supporting Pt and NiO_x structure. We further prepared Pt-NiO_x/$LaCO_3OH$ catalyst to verify it. Combining with temperature programmed surface reaction, a possible mechanism is proposed. The transformed catalyst possessed more metallic Pt sites and more abundant active OH groups, which are beneficial for methanol decomposition and CO shift, respectively. In addition, although the structure transformation happened for perovskite supporting Pt catalyst, it presented extremely excellent stability with only 7% loss of its highest rate of hydrogen production after 315 h on stream.

1. Introduction

Proton exchange membrane fuel cell (PEMFC) is considered as an efficient and clean power generating device which can directly convert the chemical energy stored in fuel into electric energy [1–3]. The hydrogen storage and transportation for PEMFC in a reliable way remain economic and safety challenges [4,5]. It is feasible to store hydrogen in a chemical form and release in situ through an efficient and controllable catalytic process [6–8]. Compared to other liquid organic and inorganic hydrogen carriers, methanol, which is inexpensive and readily available, can release a large amount of H_2 by reforming with water [9]. Especially, under the condition of aqueous phase reform (APR), CO at ppm level can be obtained, which is able to greatly improve the service life of fuel cell [10,11].

In general, but not universal, methanol APR reaction involves dehydrogenation of methanol and water gas shift (WGS) reaction [12]. Therefore, noble metals catalysts, especially Pt-based supported catalysts, have been widely investigated owing to their good ability of dissociating methanol and shifting CO [13–15]. In addition to noble metal, Ni also has been proven to be efficient in APR, but it would usually lead to non-negligible methane formation [16–18]. Gamma-Al_2O_3, the most commonly used support in APR, has shown excellent activity and selectivity in many kinds of biomass APR [14,19,20]. But due to its unsatisfactory hydrothermal stability, γ-Al_2O_3 would be transformed to hydrated boehmite under the condition of APR, which leads to the decrease of catalytic activity [21]. So, development of support with high catalytic performance and stability is one of key issues for APR [22]. Some supports with natural mineral structure, such as $NiAl_2O_4$ spinel, have been found as a stable and excellent support for APR of methanol [23].

In addition to spinel, perovskite oxides with general molecular formula ABO_3 also have excellent thermal stability [24–28], and have been reported to be used in APR reaction as support. For instance, $LaAlO_3$ perovskite supporting Ni catalyst has been revealed to be beneficial to improve the activity and stability of glycerol APR [29]. The Pt-supported perovskites also showed higher activity in APR of glycerol than Pt/γ-Al_2O_3 [30]. Nevertheless, for perovskite oxides, different degrees of B-site metal exsolution and phase transformation were found during the reforming reaction [18,30]. It seems to inevitably generate $LaCO_3OH$ for most supported perovskite oxides, which possibly depends on the cosegregation energy of B-site metal [31]. Therefore, which of perovskite oxides or metal oxides/$LaCO_3OH$ actually worked in APR is vague.

In this work, considering the higher cosegregation energy of Ni than other common B-site metal [31], two kinds of $LaNiO_x$ perovskite

* Corresponding author.
E-mail address: guoyong@ecust.edu.cn (Y. Guo).

https://doi.org/10.1016/j.apcatb.2022.121435
Received 23 January 2022; Received in revised form 2 April 2022; Accepted 18 April 2022
Available online 21 April 2022

synthesized different methods were selected as support to observe the activity and structural changes of different perovskite structures. After loading Pt, the catalysts activity and stability in APR of methanol for hydrogen production were investigated in a fixed-bed reactor. The phase transformation of the perovskite structure was explicitly unraveled with combining analysis of powder X-ray diffraction (XRD), high resolution transmission electron microscopy (HR-TEM), X-ray photoelectron spectroscopy (XPS) and X-ray absorption spectroscopy (XAS). Temperature-programmed surface reaction (TPSR) was utilized to investigate the pathway and mechanism in APR of methanol. Pt/La-CO_3OH and Pt-NiO_x/$LaCO_3OH$ catalysts were prepared and evaluated to verify the exact catalyst in APR of methanol.

2. Experimental

2.1. Materials

Methanol, concentrated nitric acid and critic acid were bought from Shanghai Titan Technology Co., Ltd. Nickel (II) nitrate hexahydrate was purchased from Sinopharm Chemical Reagent Co., Ltd. Lanthanum nitrate hydrate, sodium carbonate, polyethylene-polypropylene glycol F127 (Mw = ~ 13,500), sodium hydroxide and resol were obtained from Shanghai Macklin Biochemical Co., Ltd. Another triblock copolymer Pluronic F127 (Mw = ~ 12,600) was purchased from Sigma Aldrich (Shanghai) Trading Co., Ltd. $Pt(NO_3)_2$ was bought from Xi'an Kaili Catalyst and Materials Co., Ltd. All the above chemicals were analytical purity and used as received.

2.2. Catalysts preparation

$LaNiO_x$-1 was prepared via a resol-assisted cationic coordinative co-assembly approach [32]. Generally, 20.0 g of Pluronic F127 (Mw = ~ 12,600) was dissolved in the mixture of 113 mL ethanol and 40 mL H_2O with stirring. Then, 36.8 g of resol solution (20 wt% ethanol solution) was dropped into it and stirred for longer 20 min. Afterward, 10 mL concentrated HNO_3 was added, followed by 4.2 g citric acid after 20 min. Subsequently, 10 mmol of $La(NO_3)_3{\cdot}6H_2O$ and 8.4 mmol Ni $(NO_3)_2{\cdot}4H_2O$ were added and stirred for 3 h to obtain a homogeneous solution. The mixture was transferred onto an evaporating dish and vaporized for 2 h at 60 °C to obtain sticky films, which was then subjected to 100 ºC for 4 h and 140 °C for 12 h to form composite films. The resulting composite films were scrapped off and calcined at 680 °C in air atmosphere for 3 h with a heating rate of 2 °C min^{-1}.

$LaNiO_x$-2 was prepared in the same way as $LaNiO_x$-1, except that F127 (Mw = ~ 13,500) from Macklin was used and the amount of citric acid added was changed to 4.5 g.

$LaCO_3OH$ was synthesized as following [33]: 0.189 g NaOH and 1.431 g Na_2CO_3 were dissolved in 30 mL H_2O. The obtained alkaline solution was added rapidly into 30 mL solution containing 0.779 g La $(NO_3)_3{\cdot}6H_2O$ under vigorous stirring. The mixture was transferred to a 100 mL Teflon autoclave bottle and maintained at 230 °C for 8 h. Finally, the precipitate was washed with deionized water and dried at 100 °C for 12 h.

Pt/$LaNiO_x$-1, Pt/$LaNiO_x$-2 and Pt/$LaCO_3OH$ catalysts were prepared via a deposition-precipitation method. In a typical case, 1.5 g support was added to 40 mL deionized water. Then 67 μL of the aqueous solution of $Pt(NO_3)_2$ with 0.15 g/mL Pt (corresponding to 1 wt% Pt) was added to the suspension and stirred for 30 min. Afterward, 1 M NaOH solution was added until the pH reached 10 and stirred for 3 h at room temperature. The precipitates were filtered and washed by deionized water until the pH was 7. Finally, the solid was dried at 100 °C for 12 h and calcined at 450 °C for 5 h in the air atmosphere.

Pt-NiO_x/$LaCO_3OH$ catalyst was prepared via an incipient wetness impregnation method. 1.5 g dried Pt/$LaCO_3OH$ was added to the aqueous solution of $Ni(NO_3)_2$ (corresponding to 10 wt% Ni). The sample was obtained after drying at 100 °C for 12 h and calcination at 450 °C for 5 h in air.

2.3. Catalysts characterizations

Power X-ray diffraction (XRD) patterns of samples were recorded on a D8 Focus diffractometer (Cu Kα1 radiation). Specific areas of all the samples were measured on a Micromeritics ASAP 2020M sorption analyzer using the Brunauer-Emmett-Teller (BET) method. After being degassed at 200 °C for 6 h, the samples were measured at − 196 °C using nitrogen as the adsorptive molecular. Inductively coupled plasma atomic emission spectrometry (ICP-AES) was used to determine the metal content by using an Agilent 725ES. High resolution transmission electron microscopy (HR-TEM) and high-angle annular dark-field *Z*-contrast images were obtained on a JEOL JEM2100F electron microscopy and Energy Disperse Spectroscopy (EDS) was conducted on an Oxford TSR energy spectrometer. X-ray photoelectron spectroscopy (XPS) was carried out on a Thermo Scientific Escalab 250Xi system with monochromatic AlKa radiation, and the results were calibrated using the C1s peak at 284.8 eV. H_2 temperature-programmed reduction (H_2-TPR) was carried out on Huasi DAS-7200 automatic chemisorption system. The samples were pretreated by purging pure argon at 150 °C for 1 h first and cooled down to room temperature. Then, the samples were heated to 800 °C with a heating rate of 10 °C min^{-1} in 10% H_2/Ar flow. X-ray absorption near edge structure (XANES) measurement was conducted at the Canadian Light Source using the Soft X-ray Micro Characterization Beamline with a selected energy window (e.g., Ni K-edge). A four-element Si drift solid state detector was equipped for the fluorescence yield measurement.

The reforming of methanol and water on the catalysts was investigated through the temperature-programmed surface reaction (TPSR) technique. Before analysis, 50 mg catalyst (40–60 mesh) were pretreated in pure H_2 for 2 h at 250 °C in a quartz tube, and then cooled down to 35 °C. The system was purged thoroughly with argon to remove the desorbed molecules. Methanol vapor was introduced into the system by means of a 30 mL min^{-1} argon flow from a bubbler until the steady signal of methanol (m/z = 31) could be observed. The test sample was then heated to 400 °C at a rate of 5 °C min^{-1} under 30 mL min^{-1} argon flow. Signal of H_2 (m/z = 2), H_2O (m/z = 18), CO (m/z = 28), CH_3OH (m/z = 31), Ar (m/z = 40), CO_2 (m/z = 44), HCOOH (m/z = 46), CH_3OOCH (m/z = 60) were recorded with an OMINI Star mass spectrometer.

2.4. Catalytic activity tests

APR of methanol was conducted in a continuous flow fixed-bed reactor with a 6 mm inner diameter. 0.3 g of catalyst with 40–60 mesh was mixed thoroughly with 0.5 g silica sand (40–60 mesh). Before the test, the catalyst was in-situ activated at 250 °C for 2 h with H_2 flow. 10 wt% of aqueous methanol solution was injected into the reactor by an HPLC pump (0.015 mL min^{-1}), which resulted in a weigh hourly space velocity (WHSV) of 2.94 h^{-1}. To ensure that methanol and water were in the liquid phase, APR of methanol was carried out at 210 °C and 2.9 MPa. The reactor effluent was separated in a phase separator and then analyzed by online gas chromatography equipped with a thermal conductivity detector (TCD) and a methanator and flame ionization detector (FID).

Carbon conversion to gas products, shorted as Conv. $_{gas}$, is adopted to evaluate the performance of catalysts, which is defined as:

$$\text{Conv.}_{gas} = \text{C atoms in gaseous product/C atoms fed into reactor} \times 100\%$$

The selectivity to gaseous carbon product (i = CO_x and CH_4) were calculated as follow:

$$\text{Sel.}_i = (\text{C atoms in product i /total C atoms in gaseous product}) \times 100\%$$

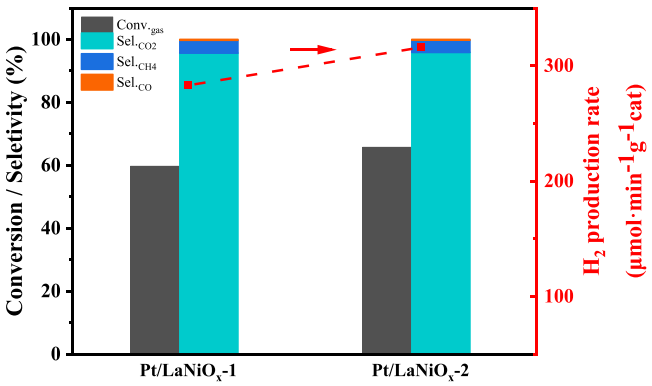

Fig. 1. Conversion, selectivity of gaseous products containing carbon and production rate of H_2 during APR of methanol (condition: 0.3 g catalyst, 10 wt % methanol aqueous solution, WHSV = 2.94 h^{-1}, 2.9 MPa, 210 °C).

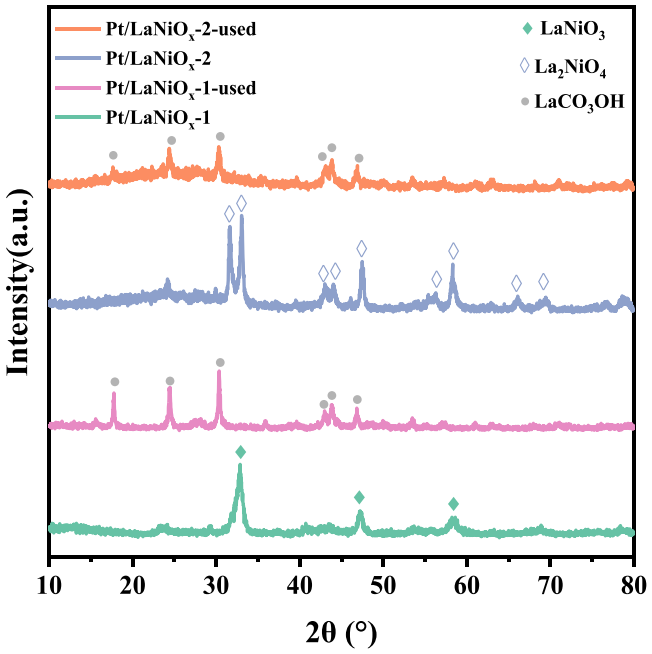

Fig. 2. XRD patterns of the fresh and used catalysts.

Y_{H2} = the determined hydrogen production rate/the theoretical hydrogen production rate × 100%

3. Results and discussion

3.1. APR of methanol over perovskite catalysts

The catalytic performance of Pt/$LaNiO_x$-1 and Pt/$LaNiO_x$-2 was evaluated firstly. Fig. 1 shows the conversion, selectivity of gaseous products containing carbon and production rate of H_2 during APR of methanol. The H_2 production rate is 315.8 μmol min^{-1} g^{-1}cat over Pt/$LaNiO_x$-2 while it is 283.0 μmol min^{-1} g^{-1}cat over Pt/$LaNiO_x$-1. The conversion of carbon to gaseous products reached 65.7% over Pt/$LaNiO_x$-2, which is little higher than that of 59.7% over Pt/$LaNiO_x$-1. There is no obvious difference in the selectivity of gaseous products between these two catalysts, either. The results show these two catalysts had a similar performance on APR of methanol, which made us suspect these two catalysts might have a similar structure during the reaction.

Table 1
Physicochemical properties of fresh and used Pt/$LaNiO_x$-1 and Pt/$LaNiO_x$-2.

Samples	S_{BET}/m^2 g^{-1}	Pt content[a]/ wt%	Ni content[a]/ wt%	La content[a]/ wt%
Pt/$LaNiO_x$-1	14.1	0.83	23	64
Pt/$LaNiO_x$-1-used	12.8	0.77	18	51
Pt/$LaNiO_x$-2	6.7	0.74	19	56
Pt/$LaNiO_x$-2-used	10.2	0.63	16	47

[a] Measured by ICP-AES.

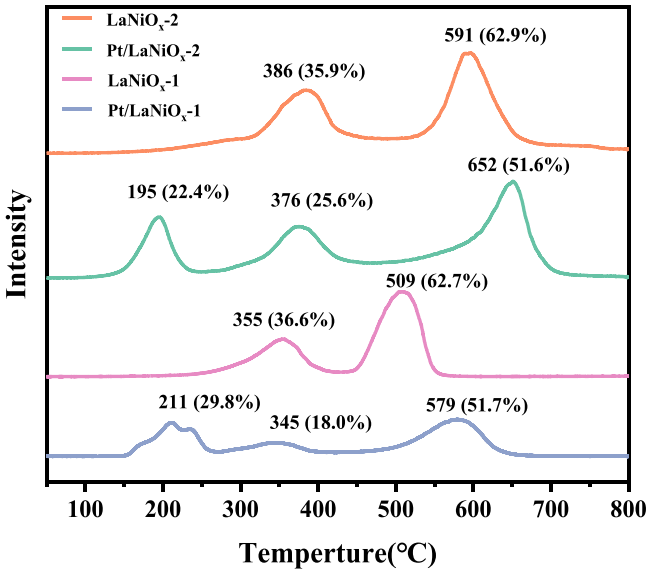

Fig. 3. H_2-TPR profiles of two supports, corresponded Pt catalysts.

3.2. The catalyst structure and reduction properties

To confirm the structure similarity of these two catalysts during the reactions, we first employed XRD characterization for the fresh and used catalysts. As presented in Fig. 2, Pt/$LaNiO_x$-1 samples obtained in this work crystallized in a rhombohedral symmetry with space group R-3 ($LaNiO_3$, PDF# 34-1077) while the Pt/$LaNiO_x$-2 samples crystallized in a tetragonal system with space group I (La_2NiO_4, PDF# 34-0984), respectively. Apparently, through different molecular weight of F127, we successfully synthesized two kinds of perovskite oxide structures, $LaNiO_3$ and La_2NiO_4. According to the obtained structure, there must be some well dispersed NiO_x species over La_2NiO_4 because Ni introduced during the synthesis of $LaNiO_x$-2 was excess and no diffraction peaks of NiO_x can be observed. Interestingly, both the used Pt/$LaNiO_x$-1 and Pt/$LaNiO_x$-2 had completely converted to the same another structure with a set of diffractions peaks at 2θ of 17.6°, 24.4°, 30.3°, 43.0°, 43.8° and 46.8°, related to the (002), (300), (302), (330), (304) and (332) planes of $LaCO_3OH$, respectively (PDF# 26-0815). It verifies that these two catalysts had the same structure during the reaction, regardless of the initial structure. In addition, there is no any diffraction peak of Ni or Pt observed in both catalysts, which could be explained by the high dispersion of Ni and the low loading of Pt.

Aforementioned catalytic results show that different perovskite structures have quite similar performance on APR of methanol. Therefore, it is critical to identify the actual structure which promotes the APR reactivity. Based on Fig. 2, both $LaNiO_x$-1 and $LaNiO_x$-2 have been converted to $LaCO_3OH$ after reaction, which could explain why the Pt, Ni and La contents of both used catalysts decreased after APR of methanol (Table 1). That is the total mass of catalyst increased as CO_2 and H_2O reacted with perovskite, leading to the decrease of their content.

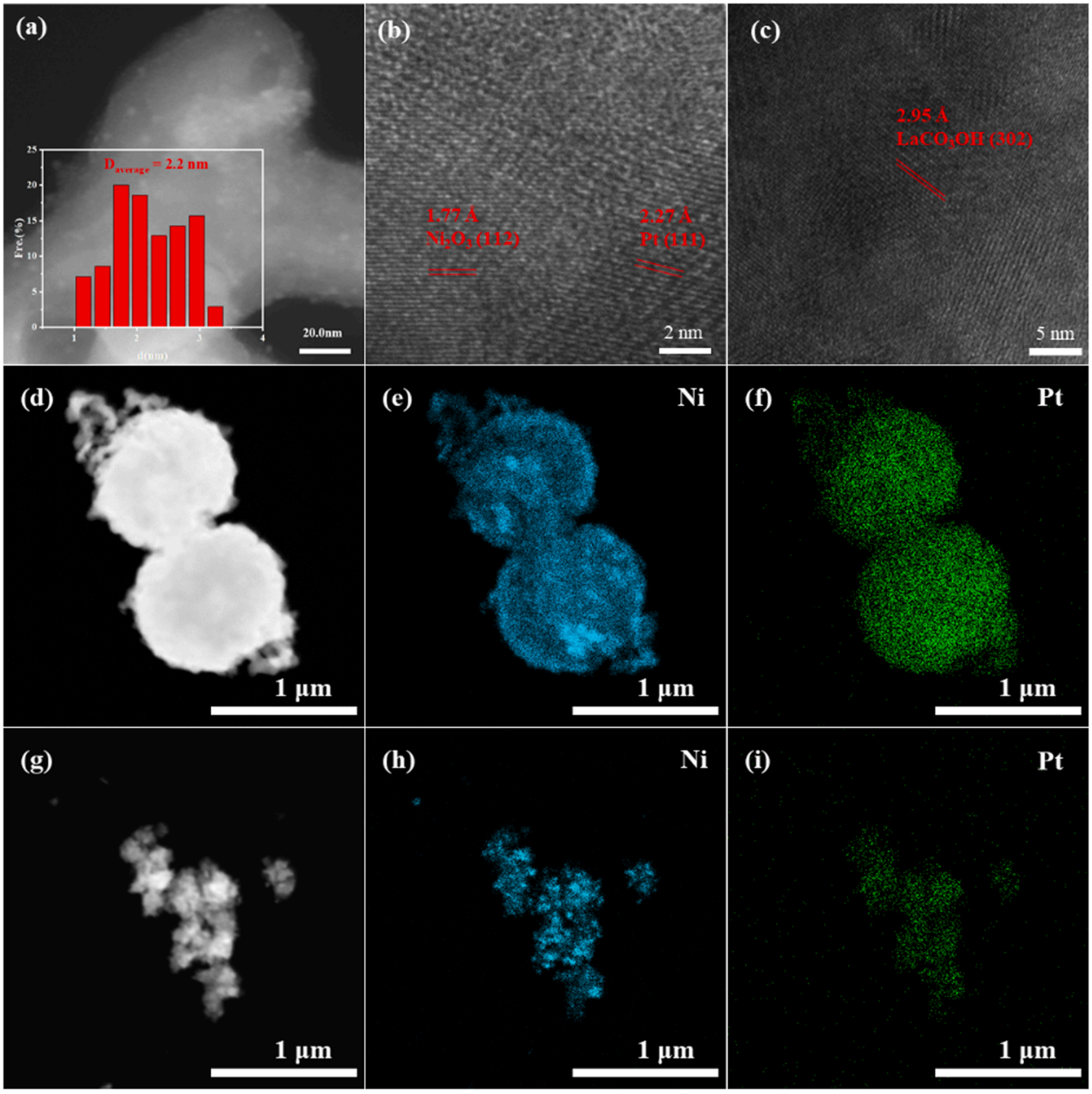

Fig. 4. TEM image of (a): Pt/$LaNiO_x$-2-reduced; HR-TEM images of (b): Pt/$LaNiO_x$-2-reduced and (c): Pt/$LaNiO_x$-2-used; (d) TEM image and the corresponding EDS elemental maps of (e) Ni and (f) Pt of Pt/$LaNiO_x$-2-reduced; (g) TEM image and the corresponding EDS elemental maps of (h) Ni and (i) Pt of Pt/$LaNiO_x$-2-used.

Owing to generation of hydrogen during APR, it may promote phase separation via reducing the catalyst in a long time. Here, H_2-TPR was employed to check the reduction behavior. As shown in Fig. 3, there are two reduction peaks for both $LaNiO_x$-1 and $LaNiO_x$-2. The peaks at 300–400 °C were perhaps resulted by the reduction of surface NiO_x species on the perovskite support [34], owing the percentage of this peak for these two perovskites is similar (36.6% vs 35.9%). The reduction peaks at above 500 °C are considered to be caused by the reduction of internal NiO_x species in the perovskite. After loading Pt, the peaks at 300–400 °C become smaller and slightly shift to lower temperature, while large peaks at around 200 °C rise. Considering the extremely low loading of Pt, we assume that the peak at around 200 °C couldn't only be ascribed the reduction of PtO_x, but also the reduction of NiO_x species which interacted strongly with Pt. It illustrates the partial NiO_x species could be segregated from perovskite lattice under the condition of APR (210 °C with H_2). This segregation led to the formation of isolated LaO_x, which could be reacted with CO_2 and H_2O more easily compared to LaO_x in perovskite. To be noticed, the peaks at above 500 °C shifted high temperature. It might be explained by more isolated LaO_x formed (near 50% of NiO_x species were reduced below 400 °C) after introducing Pt and the isolated LaO_x covered the internal NiO_x species, leading the inhibition of active hydrogen species spilling from surface to interior.

3.3. *The state of Pt and Ni species*

To figure out the variation of catalysts during APR of methanol and

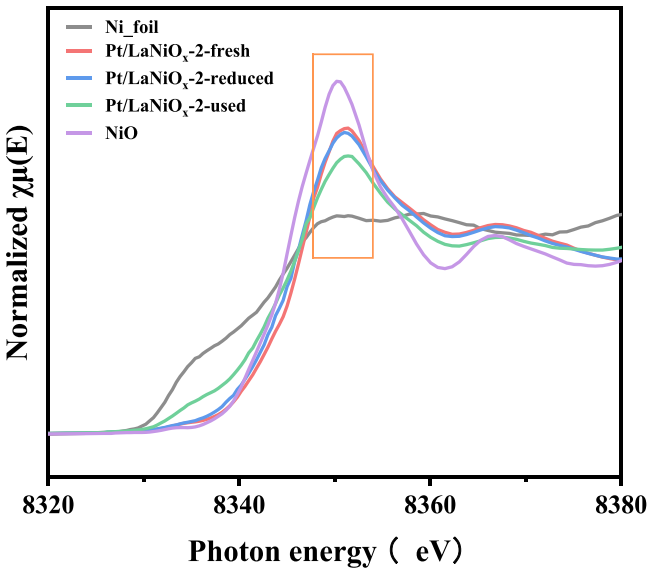

Fig. 5. Ni K-edge XANES spectra of fresh, reduced and used Pt/LaNiO$_x$-2, Ni foil and NiO.

these two catalysts showed similar performance, we chose only Pt/LaNiO$_x$-2 to carry out the following research. The fresh, reduced and spent Pt/LaNiO$_x$-2 catalysts were characterized by TEM, XPS, XANES. The TEM image of Pt/LaNiO$_x$-2-reduced is presented in Fig. 4(a). The particles of Pt are uniform and well dispersed, with an average size of ca. 2.2 nm. As shown in Fig. 4(b), it displays characteristic spacings of 2.27 Å and 1.77 Å, which are ascribed to the (111) lattice planes of Pt and (112) lattice planes of Ni_2O_3, respectively. Although H_2-TPR profiles reveal that the NiO$_x$ species could be reduced at a low temperature due to strong interaction with Pt, there is no metallic Ni species that could be found from TEM, which might be explained by two factors, one is NiO$_x$ could not be reduced to metallic Ni under this reduction condition and the other is the sample was re-oxidized during TEM analysis. After APR of methanol, an interplanar spacing of 2.95 Å for lattice planes (302) of $LaCO_3OH$ is observed in Fig. 4c, which is in line with XRD results of LaNiO$_x$-2. It further confirms the change of crystal structure. The TEM image and the corresponding Energy Disperse Spectroscopy (EDS) mappings of reduced and used Pt/LaNiO$_x$-2 are presented in Fig. 4(d–i), respectively. Pt dispersed on the supports well both before and after APR of methanol. Before reaction, Ni was rich near the surface of the catalyst, while it got more dispersed after reaction. Clearly, the morphology of catalysts also changed greatly during APR of methanol in Figs. 4(d) and 4(g).

To comprehensively assess Ni states in Pt/LaNiO$_x$-2 at different stages, Ni K-edge XANES spectrum was collected for fresh, reduced and used Pt/LaNiO$_x$-2 catalysts, Ni foil and NiO. In general, a large ‘white line’ reveals the more oxidized Ni, whereas a small one and at the lower energy refers to the reduced state of Ni species [35,36]. As shown in Fig. 5, the Ni species in fresh and reduced Pt/LaNiO$_x$-2 show almost the same ‘white line’ while that in Pt/LaNiO$_x$-2-used catalyst have a small ‘white line’ and are closer to Ni foil. These results indicate that most Ni species in Pt/LaNiO$_x$-2 cannot be reduced to metallic Ni at 250 °C, likely due to the solid structure of perovskite. Interestingly, during APR of methanol, Ni species could be reduced with a deeper degree at just 210 °C, which further reveals the segregation occurred.

X-ray photoelectron spectroscopy (XPS) analysis was carried out to clarify the state of oxygen species and Pt. The XPS of spectra of reduced and used samples were recorded and presented in Fig. 6. The O 1s orbital shows a significant difference between reduced and used samples. The spectrum for Pt/LaNiO$_x$-2-reduced can be fit into four distinct oxygen peaks corresponding to lattice oxygen in lanthanum oxide (528.2 eV) and nickel oxide (530.4 eV), lanthanum and nickel hydroxides (531.3 eV), and adsorbed oxygen species (532.8 eV) [37,38]. Rare earth oxides easily become hydroxides when exposed to aqueous conditions [39] (here H_2O was generated during the reduction with H_2). As a consequence, the area of hydroxides species exceeds that of lattice oxygen species. After reaction, three different oxygen species referring to lattice oxygen in lanthanum carbonate (531.1 eV), OH groups (532.1 eV) and adsorbed water (533.0 eV) are observed. Clearly, the peak of oxygen species ascribed to lanthanum oxide (528.2 eV) and nickel oxide (530.4 eV) disappeared, due to the phase transition of perovskite structure and the reduction of nickel oxide near the surface (Fig. 5). The binding energy for OH groups in the used catalyst is 0.8 eV higher than the reduced catalyst and the peak is wider, which reveals it perhaps contained another oxygen species except for hydroxides, such as adsorbed OH in deficient sites. Generally, these oxygen species possess less electronics. Moreover, these oxygen species have been proved to be highly beneficial to APR reaction [22]. Anyhow, the changes of oxygen species observed from XPS could ulteriorly illustrate the segregation of perovskite structure during the reaction.

The valence of Pt has great influence on APR reaction and generally the metallic Pt is favorable. There are two peaks at 70.9 eV and 71.9 eV in the curve of Pt $4f_{5/2}$ orbital for the reduced Pt/LaNiO$_x$-2 (Fig. 6b), which were assigned to Pt^0 and Pt^{2+} species, respectively [40,41]. Interestingly, the XPS spectrum of the used Pt/LaNiO$_x$-2 only shows metallic Pt^0 species at the typical B.E. of 71.0 eV, which should be responsible for its good performance. As literature reporting, the peak splitting of La $3d_{5/2}$ can distinguish the different species of La [42]. The splitting is 3.6 eV for $La(OH)_3$ [43] and 4.1 eV for $La_2O_2(CO_3)_3$ [44], which is close to our results of La $3d_{5/2}$ for reduced and used Pt/LaNiO$_x$-2, respectively (Fig. 6c). The reduced sample was exposed to air and became hydroxides to form $La(OH)_3$ on the surface while after reaction the formation of carbonate forced the splitting to 4.0 eV, which is consistent with the O 1s spectrum.

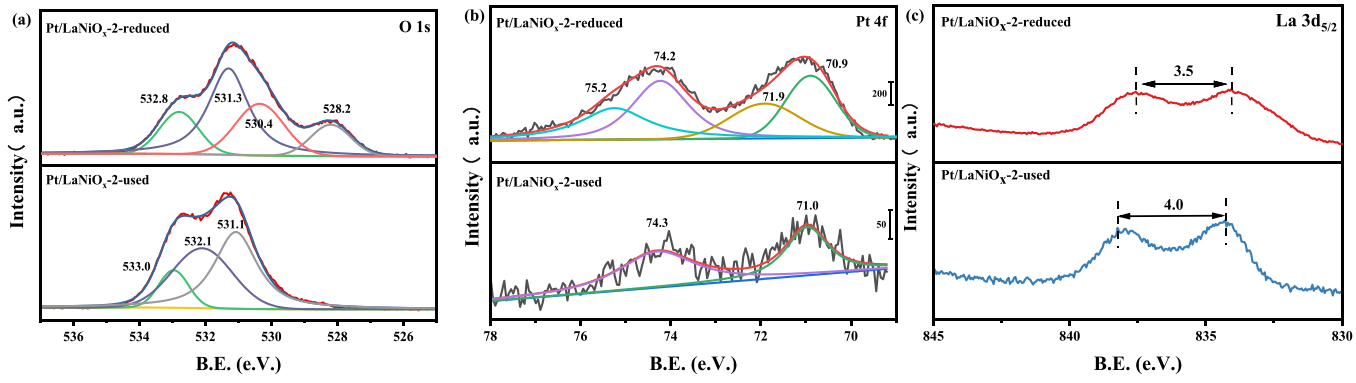

Fig. 6. XPS of reduced and used Pt/LaNiO$_x$-2, a: O 1s, b: Pt 4f, c: La $3d_{5/2}$.

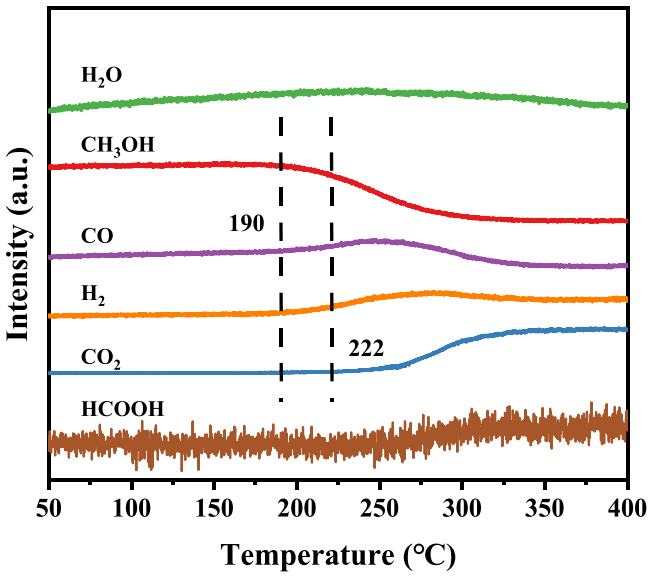

Fig. 7. Temperature-programmed surface reaction (TPSR) of methanol and water over Pt/LaNiO$_x$-2-used.

3.4. TPSR of methanol APR

There are several reaction mechanisms for methanol reforming [45]. One is the path with methanol decomposition and water gas shift reaction, that methanol is directly decomposed to CO and H_2, and then CO shifts with water to CO_2 and H_2 [14]. Another is the path without CO intermediate involved, i.e., methanol is only dehydrogenized to HCHO rather than completely to CO. The intermediate formaldehyde will react with H_2O or CH_3O·and generate formate or methyl formate, which could decompose to CO_2 and H_2 [46–48]. In the former path, the water gas shift reaction can undergo via either associative mechanism or redox mechanism [49–51]. Therefore, temperature-programmed surface reaction (TPSR) study was employed to identify the possible intermediates and reaction pathway. In our catalytic system, as shown in Fig. 7, methanol started to be consumed at 190 °C accompanying the generation of CO and H_2, indicating that CO is the intermediate product on Pt/LaNiO$_x$-2-used. After the increasing temperature to 222 °C, the signals of HCOOH and CO_2 came out very closely one after another, suggesting WGS reaction underwent via the associative mechanism. In this mechanism, the activation and dissociation of H_2O to OH group is considered to be crucial [52,53]. According to the characterization of catalyst, the abundant existence of absorbed OH groups on deficient sites may play this crucial rule, owing these OH groups are usually considered to possess higher activity.

3.5. Stability and the realistic catalyst

Stability is another important factor for application of catalyst. Here, we conducted a 315 h long-term stability test over Pt/LaNiO$_x$-2 and the result is displayed in Fig. 8a. Pt/LaNiO$_x$-2 exhibited excellent stability. The production rate of H_2 LaNiO$_x$-2 was kept at 93% of its highest value after 315 h on stream. Considering the change of catalyst during the reaction, we have hypothesized the real catalyst should be $LaCO_3OH$ supporting Pt or NiO$_x$-Pt. To certify the hypothesis, we synthesized $LaCO_3OH$ as support and loaded Pt or Pt-NiO$_x$ to obtain Pt/$LaCO_3OH$ or

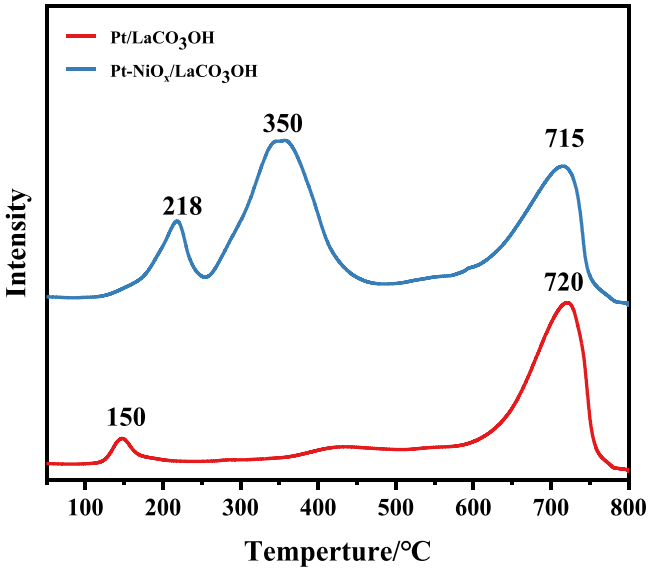

Fig. 9. H_2-TPR profiles of Pt/$LaCO_3OH$ and Pt-NiO$_x$/$LaCO_3OH$.

Table 2
Performance of methanol APR over Pt/LaNiO$_x$-1, Pt/LaNiO$_x$-2, Pt/$LaCO_3OH$ and Pt-NiO$_x$/$LaCO_3OH$.

Catalysts	Conv.$_{gas}$/ %	Conc.$_{CO}$/ ppm/%	Sel.$_{CH4}$/ %	Sel.$_{CO2}$/ %	Y$_{H2}$/ %
Pt/LaNiO$_x$-1@69 h	59.7	0.2	4.1	95.7	57.1
Pt/LaNiO$_x$-2@110 h	64.6	0.2	2.8	97.0	66.6
Pt/LaNiO$_x$-2@315 h	62.6	0.2	2.6	97.2	62.0
Pt/$LaCO_3OH$	13.6	0.1	0.4	99.5	13.3
Pt-NiO$_x$/ $LaCO_3OH$	62.0	0.2	2.4	97.4	57.6

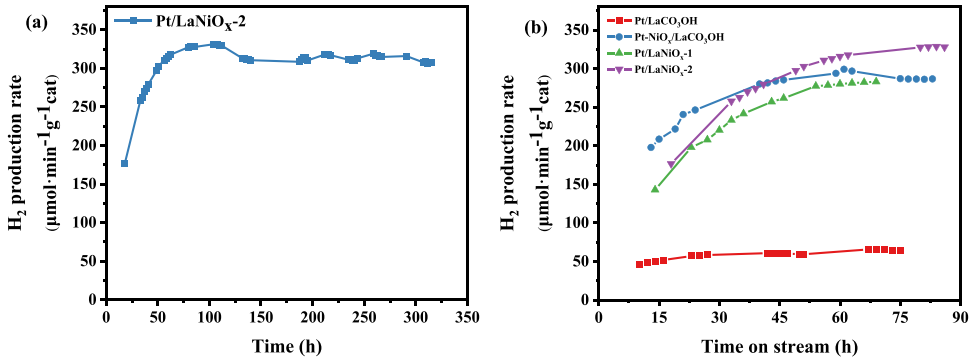

Fig. 8. a: Long-term test for H_2 production over Pt/LaNiO$_x$-2, b: Time on stream for H_2 production over Pt/LaNiO$_x$-1, Pt/LaNiO$_x$-2, Pt/$LaCO_3OH$ and Pt-NiO$_x$/$LaCO_3OH$ (Reaction condition: 0.3 g catalyst 10 wt% methanol/water, WHSV = 2.94 h^{-1}, 2.9 MPa, 210 °C).

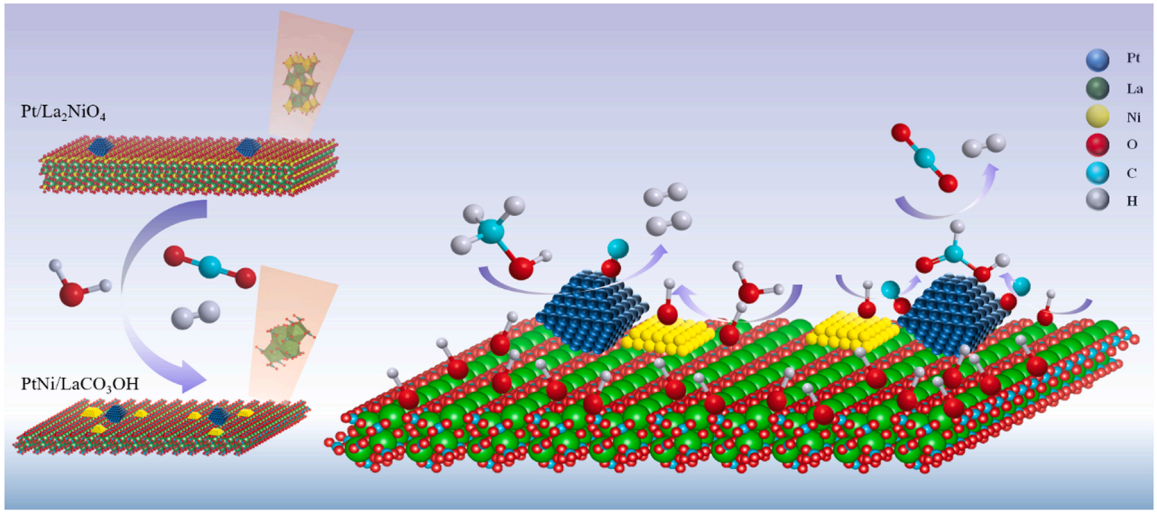

Scheme 1. Structure change of Pt/LaNiO_x-2 during APR of methanol and schematic illustrations of mechanism of methanol APR.

Pt-NiO_x/LaCO_3OH catalyst. The H_2-TPR profiles of Pt/LaCO_3OH and Pt-NiO_x/LaCO_3OH are shown in Fig. 9. The reduction peaks at the approximately 700 °C are attributed to the decomposition of carbonates. The reduction peak of Pt appeared at 150 °C for Pt/LaCO_3OH. After introducing NiO_x, it shifted to a high reduction temperature of 218 °C, indicating the existence of strong interaction between Pt and NiO_x, which is consistent with the above results and discussions. Their catalytic performance is shown in Fig. 8b and listed in Table 2. Pt/LaCO_3OH showed poor performance for APR of methanol, while Pt-NiO_x/LaCO_3OH presented nearly the same performance as Pt/LaNiO_x-2, indicating that our hypothesis is rationale.

On the basis of the present results, we have proven that lanthanum nickel perovskite supporting Pt catalyst would change the original perovskite structure to another one Pt-NiO_x/LaCO_3OH during APR of methanol, as shown in Scheme 1. Combining the results of this work and previous works [52,53], we propose one possible reaction mechanism of methanol APR over the catalyst of lanthanum nickel perovskite supporting Pt. APR of methanol over this catalyst undergoes methanol decompose to CO and H_2, followed by WGS reaction to generate CO_2 and H_2. Specifically, methanol is decomposed on metallic Pt sites to generate adsorbed *CO intermediate, which could be shifted by OH groups adsorbed on lanthanum or nickel to form formate species. Thus, the metallic Pt sites are recovered. The consumed OH groups are supplemented by adsorbing/dissociating H_2O on lanthanum and nickel species. Ultimately, formate intermediates converted to H_2 and CO_2.

4. Conclusion

In this work, we synthesized two lanthanum nickel perovskite oxides with different perovskite and loaded Pt (Pt/LaNiO_x-1 and Pt/LaNiO_x-2) to obtain corresponding catalysts. These two catalysts showed similar catalytic performance on APR of methanol. Detailed investigations revealed that these two perovskite catalysts transformed into LaCO_3OH supporting Pt and NiO_x structure, so they displayed similar catalytic properties. Pt-NiO_x/LaCO_3OH catalyst was further prepared and displayed the similar catalytic performance with Pt/LaNiO_x-2, verifying the realistic catalyst is Pt-NiO_x/LaCO_3OH. The transformed catalyst possessed more metallic Pt sites and more abundant active OH groups, which are beneficial for methanol dehydration and CO shift, respectively. Mechanism study indicates that APR of methanol has occurred through decompose of methanol to CO and the following WGS reaction. Even more, WGS reaction has undergone in the associative mechanism to form formate intermediate, in which the role of OH species on catalyst is crucial. Additionally, although the structure transformation happened for lanthanum nickel perovskite supporting Pt catalyst during the reaction, it presented extremely excellent stability with only 7% loss of its highest rate of hydrogen production after 315 h on stream, which is one of the most stable catalysts has been reported. This study reveals a deep understanding into the structure transformation of perovskite oxide catalyst and its mechanism towards efficient and stable production of hydrogen via APR of methanol.

CRediT authorship contribution statement

Qianlong Mao: Investigation, Data curation, Writing – original draft. **Yong Guo:** Conceptualization, Writing – review & editing, Supervision, Funding acquisition. **Xiaohui Liu:** Investigation, Data curation, Writing – original draft. **Mohsen Shakouri:** Investigation. **Yongfeng Hu:** Investigation, Writing – review & editing. **Yanqin Wang:** Writing – review & editing, Supervision, Funding acquisition.

Declaration of Competing Interest

The authors declare that they have no known competing financial interests or personal relationships that could have appeared to influence the work reported in this paper.

Acknowledgements

This work was supported financially by the NSFC of China (Nos. 22072041, 21832002, 21808063, 21872050), and the Science and Technology Commission of Shanghai Municipality (10dz2220500). We thank Canadian Light Source Inc. for the help at characterization of XANES.

References

[1] B.C.H. Steele, A. Heinzel, Materials for fuel-cell technologies, Nature 414 (2001) 345–352.
[2] A. Serov, C. Kwak, Review of non-platinum anode catalysts for DMFC and PEMFC application, Appl. Catal. B 90 (2009) 313–320.
[3] Y. Shao, J. Sui, G. Yin, Y. Gao, Nitrogen-doped carbon nanostructures and their composites as catalytic materials for proton exchange membrane fuel cell, Appl. Catal. B 79 (2008) 89–99.
[4] Z.-Y. Deng, J.M.F. Ferreira, Y. Sakka, Hydrogen-generation materials for portable applications, J. Am. Chem. Soc. 91 (2008) 3825–3834.
[5] A.M. Seayad, D.M. Antonelli, Recent advances in hydrogen storage in metal-containing inorganic nanostructures and related materials, Adv. Mater. 16 (2004) 765–777.
[6] T.W. Kim, M. Kim, S.K. Kim, Y.N. Choi, M. Jung, H. Oh, Y.-W. Suh, Remarkably fast low-temperature hydrogen storage into aromatic benzyltoluenes over MgO-

supported Ru nanoparticles with homolytic and heterolytic H_2 adsorption, Appl. Catal. B 286 (2021).
[7] B. Wang, Y.-T. Chen, T.-Y. Chang, Z. Jiang, Z.-Q. Huang, S.-Y. Wang, C.-R. Chang, Y.-S. Chen, J.-J. Wei, S. Yang, T. Fang, Facet-dependent catalytic activities of Pd/rGO: exploring dehydrogenation mechanism of dodecahydro-N-ethylcarbazole, Appl. Catal. B 266 (2020).
[8] B. Wang, T.-y Chang, Z. Jiang, J.-j Wei, T. Fang, Component controlled synthesis of bimetallic PdCu nanoparticles supported on reduced graphene oxide for dehydrogenation of dodecahydro-N-ethylcarbazole, Appl. Catal. B 251 (2019) 261–272.
[9] D.R. Palo, R.A. Dagle, J.D. Holladay, Methanol steam reforming for hydrogen production, Chem. Rev. 107 (2007) 3992–4021.
[10] R.D. Cortright, R.R. Davda, J.A. Dumesic, Hydrogen from catalytic reforming of biomass-derived hydrocarbons in liquid water, Nature 418 (2002) 964–967.
[11] G.W. Huber, J.W. Shabaker, J.A. Dumesic, Raney Ni-Sn catalyst for H_2 production from biomass-derived hydrocarbons, Science 300 (2003) 2075–2077.
[12] L. Lin, Q. Yu, M. Peng, A. Li, S. Yao, S. Tian, X. Liu, A. Li, Z. Jiang, R. Gao, X. Han, Y.W. Li, X.D. Wen, W. Zhou, D. Ma, Atomically dispersed Ni/α-MoC catalyst for hydrogen production from methanol/water, J. Am. Chem. Soc. 143 (2021) 309–317.
[13] L. Lin, W. Zhou, R. Gao, S. Yao, X. Zhang, W. Xu, S. Zheng, Z. Jiang, Q. Yu, Y.W. Li, C. Shi, X.D. Wen, D. Ma, Low-temperature hydrogen production from water and methanol using Pt/α-MoC catalysts, Nature 544 (2017) 80–83.
[14] J. Callison, N.D. Subramanian, S.M. Rogers, A. Chutia, D. Gianolio, C.R.A. Catlow, P.P. Wells, N. Dimitratos, Directed aqueous-phase reforming of glycerol through tailored platinum nanoparticles, Appl. Catal. B 238 (2018) 618–628.
[15] A. Ciftci, D.A.J.M. Ligthart, E.J.M. Hensen, Influence of Pt particle size and Re addition by catalytic reduction on aqueous phase reforming of glycerol for carbon-supported Pt(Re) catalysts, Appl. Catal. B 174 (2015) 126–135.
[16] R.R. Davda, J.W. Shabaker, G.W. Huber, R.D. Cortright, J.A. Dumesic, Aqueous-phase reforming of ethylene glycol on silica-supported metal catalysts, Appl. Catal. B 43 (2003) 13–26.
[17] A. Morales-Marín, J.L. Ayastuy, U. Iriarte-Velasco, M.A. Gutiérrez-Ortiz, Nickel aluminate spinel-derived catalysts for the aqueous phase reforming of glycerol: effect of reduction temperature, Appl. Catal. B 244 (2019) 931–945.
[18] A. Arandia, I. Coronado, A. Remiro, A.G. Gayubo, M. Reinikainen, Aqueous-phase reforming of bio-oil aqueous fraction over nickel-based catalysts, Int. J. Hydrog. Energy 44 (2019) 13157–13168.
[19] F. Bastan, M. Kazemeini, A. Larimi, H. Maleki, Production of renewable hydrogen through aqueous-phase reforming of glycerol over Ni/Al_2O_3-MgO nano-catalyst, Int. J. Hydrog. Energy 43 (2018) 614–621.
[20] Y. Kim, M. Kim, H. Jeong, Y. Kim, S.H. Choi, H.C. Ham, S.W. Lee, J.Y. Kim, K. H. Song, C.W. Yoon, Y.S. Jo, H. Sohn, High purity hydrogen production via aqueous phase reforming of xylose over small Pt nanoparticles on a γ-Al_2O_3 support, Int. J. Hydrog. Energy 45 (2020) 13848–13861.
[21] R.M. Ravenelle, J.R. Copeland, W.-G. Kim, J.C. Crittenden, C. Sievers, Structural changes of γ-Al_2O_3-supported catalysts in hot liquid water, Acs Catal. 1 (2011) 552–561.
[22] D. Li, Y. Li, X. Liu, Y. Guo, C.-W. Pao, J.-L. Chen, Y. Hu, Y. Wang, $NiAl_2O_4$ spinel supported Pt catalyst: high performance and origin in aqueous-phase reforming of methanol, ACS Catal. 9 (2019) 9671–9682.
[23] A.J. Reynoso, J.L. Ayastuy, U. Iriarte-Velasco, M.A. Gutierrez-Ortiz, E. Chemical Technologies, Cobalt aluminate spinel-derived catalysts for glycerol aqueous phase reforming, Appl. Catal. B 239 (2018) 86–101.
[24] R. Huang, C. Lim, M.G. Jang, J.Y. Hwang, J.W. Han, Exsolved metal-boosted active perovskite oxide catalyst for stable water gas shift reaction, J. Catal. 400 (2021) 148–159.
[25] B. Levasseur, S. Kaliaguine, Methanol oxidation on $LaBO_3$ (B = Co, Mn, Fe) perovskite-type catalysts prepared by reactive grinding, Appl. Catal. A 343 (2008) 29–38.
[26] H. Wang, R. Zhang, P. Li, S. Royer, J.-P. Dacquin, Mechanistic insight into the methanol selective catalytic reduction of NO reaction over Cu-containing perovskites, J. Catal. 377 (2019) 480–493.
[27] F.S. Toniolo, R.N.S.H. Magalhaes, C.A.C. Perez, M. Schmal, Structural investigation of LaCoO3 and LaCoCuO3 perovskite-type oxides and the effect of Cu on coke deposition in the partial oxidation of methane, Appl. Catal. B 117 (2012) 156–166.
[28] G. Wu, S. Li, C. Zhang, T. Wang, J. Gong, Glycerol steam reforming over perovskite-derived nickel-based catalysts, Appl. Catal. B 144 (2014) 277–285.
[29] Y.H. Park, J.Y. Kim, D.J. Moon, N.C. Park, Y.C. Kim, Effect of $LaAlO_3$-supported modified Ni-based catalysts on aqueous phase reforming of glycerol, Res. Chem. Intermed. 41 (2015) 9603–9614.
[30] D.R. Inns, A.J. Mayer, V. Skukauskas, T.E. Davies, J. Callison, S.A. Kondrat, Evaluating the activity and stability of perovskite $LaMO_3$-based Pt catalysts in the aqueous phase reforming of glycerol, Top. Catal. (2021).
[31] S. Joo, A. Seong, O. Kwon, K. Kim, J.H. Lee, R.J. Gorte, J.M. Vohs, J.W. Han, G. Kim, Highly active dry methane reforming catalysts with boosted in situ grown Ni-Fe nanoparticles on perovskite via atomic layer deposition, Sci. Adv. 6 (2020).
[32] Y. Zheng, R. Zhang, L. Zhang, Q. Gu, Z.A. Qiao, A resol-assisted cationic coordinative Co-assembly approach to mesoporous ABO_3 perovskite oxides with rich oxygen vacancy for enhanced hydrogenation of furfural to furfuryl alcohol, Angew. Chem. Int. Ed. 60 (2021) 4774–4781.
[33] Y. Zhang, K. Han, T. Cheng, Z. Fang, Synthesis, characterization, and photoluminescence property of $LaCO_3OH$ microspheres, Inorg. Chem. 46 (2007) 4713–4717.
[34] R. Pereniguez, V.M. Gonzalez-DelaCruz, J.P. Holgado, A. Caballero, Synthesis and characterization of a $LaNiO_3$ perovskite as precursor for methane reforming reactions catalysts, Appl. Catal. B 93 (2010) 346–353.
[35] D.B.L. Santos, F.B. Noronha, C.E. Hori, Bi-reforming of methane for hydrogen production using $LaNiO_3/Ce_xZr_{1-x}O_2$ as precursor material, Int. J. Hydrog. Energy 45 (2020) 13947–13959.
[36] S. Bepari, D. Kuila, Steam reforming of methanol, ethanol and glycerol over nickel-based catalysts–a review, Int. J. Hydrog. Energy 45 (2020) 18090–18113.
[37] W.G. Hardin, D.A. Slanac, X. Wang, S. Dai, K.P. Johnston, K.J. Stevenson, Highly active, nonprecious metal perovskite electrocatalysts for bifunctional metal-air battery electrodes, J. Phys. Chem. Lett. 4 (2013) 1254–1259.
[38] J. Choisnet, N. Abadzhieva, P. Stefanov, D. Klissurski, J.M. Bassat, V. Rives, L. Minchev, X-ray photoelectron spectroscopy, temperature-programmed desorption and temperature-programmed reduction study of $LaNiO_3$ and $La_2NiO_{4+\delta}$ catalysts for methanol oxidation, J. Chem. Soc. Faraday Trans. 90 (1994) 1987–1991.
[39] K.N. Jung, J.H. Jung, W.B. Im, S. Yoon, K.H. Shin, J.W. Lee, Doped lanthanum nickelates with a layered perovskite structure as bifunctional cathode catalysts for rechargeable metal-air batteries, ACS Appl. Mater. Interfaces 5 (2013) 9902–9907.
[40] K. Gao, M. Wei, Z. Qu, Q. Fu, X. Bao, Dynamic STructural Changes of Perovskite-supported Metal Catalysts during Cyclic Redox Treatments and Effect on Catalytic CO oxidation, Chin. J. Catal. 34 (2013) 889–897.
[41] T. Rajesh, A.K. Rajarajan, C.S. Gopinath, R.N. Devi, Evidence of cationic Pt active for water–gas shift reaction: Pt-doped $BaCeO_3$ perovskite, J. Phys. Chem. C 116 (2012) 9526–9532.
[42] J.P.H. Li, X. Zhou, Y. Pang, L. Zhu, E.I. Vovk, L. Cong, A.P. van Bavel, S. Li, Y. Yang, Understanding of binding energy calibration in XPS of lanthanum oxide by in situ treatment, Phys. Chem. Chem. Phys. 21 (2019) 22351–22358.
[43] J.-G. Kang, Y.-I. Kim, D. Won Cho, Y. Sohn, Synthesis and physicochemical properties of $La(OH)_3$ and La_2O_3 nanostructures, Mater. Sci. Semicond. Process. 40 (2015) 737–743.
[44] T. Jiang, J. Song, M. Huo, N. Yang, J. Liu, J. Zhang, Y. Sun, Y. Zhu, La_2O_3 catalysts with diverse spatial dimensionality for oxidative coupling of methane to produce ethylene and ethane, Rsc Adv. 6 (2016) 34872–34876.
[45] S. Sa, H. Silva, L. Brandao, J.M. Sousa, A. Mendes, Catalysts for methanol steam reforming–a review, Appl. Catal. B 99 (2010) 43–57.
[46] J. Cao, Y. Ma, G. Guan, X. Hao, X. Ma, Z. Wang, K. Kusakabe, A. Abudula, Reaction intermediate species during the steam reforming of methanol over metal modified molybdenum carbide catalysts, Appl. Catal. B 189 (2016) 12–18.
[47] N. Yi, R. Si, H. Saltsburg, M. Flytzani-Stephanopoulos, Steam reforming of methanol over ceria and gold-ceria nanoshapes, Appl. Catal. B 95 (2010) 87–92.
[48] J. Papavasiliou, G. Avgouropoulos, T. Ioannides, Steady-state isotopic transient kinetic analysis of steam reforming of methanol over Cu-based catalysts, Appl. Catal. B 88 (2009) 490–496.
[49] J.L.C. Fajin, M. Natalia, D.S. Cordeiro, Probing the efficiency of platinum nanotubes for the H_2 production by water gas shift reaction: a DFT study, Appl. Catal. B 263 (2020).
[50] C.M. Kalamaras, K.C. Petallidou, A.M. Efstathiou, The effect of La^{3+}-doping of CeO_2 support on the water-gas shift reaction mechanism and kinetics over Pt/$Ce_{1-x}La_xO_{2-\delta}$, Appl. Catal. B 136 (2013) 225–238.
[51] K.G. Azzam, I.V. Babich, K. Seshan, L. Lefferts, Role of Re in Pt-Re/TiO_2 catalyst for water gas shift reaction: a mechanistic and kinetic study, Appl. Catal. B 80 (2008) 129–140.
[52] Y. Guo, M.U. Azmat, X.H. Liu, Y.Q. Wang, G.Z. Lu, Effect of support's basic properties on hydrogen production in aqueous-phase reforming of glycerol and correlation between WGS and APR, Appl. Energy 92 (2012) 218–223.
[53] Y. Guo, X.H. Liu, Y.Q. Wang, Catalytic and DRIFTS studies of Pt-based bimetallic alloy catalysts in aqueous-phase reforming of glycerol, Ind. Eng. Chem. Res. 58 (2019) 2749–2758.